Nuclear Instruments and Methods in Physics Research B 360 (2015) 23–29

Contents lists available at ScienceDirect

Nuclear Instruments and Methods in Physics Research B

journal homepage: www.elsevier.com/locate/nimb

Proton–silicon interaction potential extracted from high-resolution measurements of crystal rainbows

S. Petrović [a,*], N. Nešković [a], M. Ćosić [a], M. Motapothula [b], M.B.H. Breese [b,c]

[a] Laboratory of Physics, Vinča Institute of Nuclear Sciences, University of Belgrade, P. O. Box 522, 11001 Belgrade, Serbia
[b] Center for Ion Beam Applications, Physics Department, National University of Singapore, Lower Kent Ridge Road, Singapore 117542, Singapore
[c] Singapore Synchrotron Light Source (SSLS), National University of Singapore, 5 Research Link, Singapore 117603, Singapore

ARTICLE INFO

Article history:
Received 20 May 2015
Received in revised form 21 July 2015
Accepted 21 July 2015

Keywords:
Ion channeling
Rainbows
Interaction potential

ABSTRACT

This study provides a way to produce very accurate ion–atom interaction potentials. We present the high-resolution measurements of angular distributions of protons of energies between 2.0 and 0.7 MeV channeled in a 55 nm thick (0 0 1) silicon membrane. Analysis is performed using the theory of crystal rainbows in which the Molière's interaction potential is modified to make it accurate both close to the channel axis and close to the atomic strings defining the channel. This modification is based on adjusting the shapes of the rainbow lines appearing in the transmission angle plane, with the resulting theoretical angular distributions of transmitted protons being in excellent agreement with the corresponding experimental distributions.

1. Introduction

Axial ion channeling is the passage of energetic ions through axial crystal channels [1–4], with their trajectories determined by the interaction with crystal atoms. The most frequently used ion–atom interaction potential in treating atomic collisions in solids is that proposed by Ziegler, Biersack & Littmark (ZBL) [5–7]. The other frequently used interaction potential in the field is that derived by Molière [8]. However, the problem of accurate determination of such a potential at small and large ion–atom distances remains acute. Its proper solution will definitively represent an important step forward in many fields, *e.g.*, it will ensure more accurate prediction of impurity concentration profiles during ion implantation processes [9–11], and enable more accurate determination of such profiles [10–12].

Using ion–molecule scattering theory, Nešković [13] and Nešković & Perović [14] developed a model of axial ion channeling in thin crystals, showing that a rainbow occurred. Analogous to scattering of sunlight from water droplets [15,16], the rainbow clearly divided the angular distribution of transmitted ions into the bright and dark parts. In Ref. [17], the model was generalized to be valid for thicker crystals as well. Thus, the theory of crystal rainbows was formulated, allowing accurate investigation of ion channeling in crystals and nanotubes [18].

2. Measurements of crystal rainbows

The crystal rainbow effect was first observed experimentally by Krause et al. [19], using protons of an energy of 7 MeV transmitted through (0 0 1) and (0 1 1) silicon crystals that were 140 and 198 nm thick, respectively. The corresponding values of the reduced crystal thickness, defined as $\Lambda = f_k L/v_0$, where L is the crystal thickness, v_0 the initial ion velocity, and f_k the frequency of ion motion close to the channel axis, were 0.23 and 0.24, respectively. Since both values of Λ were below 0.25, when a majority of ions make less than a quarter of an oscillation around the channel center, the results were analyzed and interpreted using the model of crystal rainbows [13,14]. The authors used the Lindhard's interaction potential [2].

The same group performed another measurement of crystal rainbows [20], using 2–9 MeV protons and 6–30 MeV C^{4+}, C^{5+} and C^{6+} ions transmitted through 179 and 190 nm thick (0 0 1) silicon crystals. For protons, the corresponding values of Λ were from 0.29 to 0.66, and for carbon ions, they were from 0.29 to 0.85. The results were successfully explained using the LAROSE three-dimensional simulation code [3,21] with the Molière's interaction potential [8]. The authors also analyzed the periodicity of evolution of the whole angular distribution of channeled ions and found that it could be investigated with respect to Λ, in spite of the fact that the parameter was determined from the second-order terms of the Taylor expansion of the ion–crystal continuum interaction potential close to the axis. They concluded that

* Corresponding author.
E-mail address: petrovs@vinca.rs (S. Petrović).

http://dx.doi.org/10.1016/j.nimb.2015.07.104
0168-583X/

the evolution of the angular distribution was to be divided into cycles. The first cycle lasts for Λ between 0 and 0.5, the second cycle for Λ between 0.5 and 1, and so on.

However, in both experiments, the measurement resolution was not sufficiently high to observe fine structure of the angular distributions of transmitted ions due to inability to provide thinner silicon crystals. Recently, a new silicon crystal fabrication process enabled the production of ultra-thin (001) silicon membranes of a thickness of 55 nm with a surface roughness of 0.4 nm [22]. Those membranes were used in the high-resolution channeling measurements with a 2.0 MeV proton microbeam to study the crystal rainbow effect as well as the doughnut effect [22–25] for the major crystallographic directions. The corresponding value of Λ along the [001] direction was 0.12. The same procedure was used to measure the channeling patterns for the minor crystallographic directions [26]. The results were analyzed using the FLUX three-dimensional simulation code [27,28] with the ZBL interaction potential [5–7]. The code uses the binary collision approximation and accounts for the thermal vibrations of crystal atoms and the collisions of protons with crystal electrons.

3. Theory of crystal rainbows

Let us now briefly describe the relevant part of the theory of crystal rainbows [17]. We consider that the z axis of the reference frame, being the longitudinal axis, coincides with the channel axis and that its origin lies in the entrance plane of the crystal. The x and y axes of the reference frame, being the transverse axes, are the vertical and horizontal axes, respectively. The initial proton velocity vectors are taken to be parallel to the channel axis. We introduce the mapping of the impact parameter (IP) plane to the transmission angle (TA) plane,

$$\theta_x = \theta_x(x_0, y_0, \Lambda) \text{ and } \theta_y = \theta_y(x_0, y_0, \Lambda), \tag{1}$$

where x_0 and y_0 are the transverse components of the initial ion position vector, *i.e.*, the components of its impact parameter vector, and θ_x and θ_y are the components of the final ion channeling angle, *i.e.*, the components of its transmission angle. To obtain θ_x and θ_y, the ion equations of motion are solved. It is assumed that the ion–crystal interaction can be treated classically [1–4]. One applies either the continuum approximation [2] or the binary collision approximation [3]. The thermal vibrations of crystal atoms can be included in the calculations.

Since the components of the ion channeling angle remain small during the whole channeling process [1–4], the ion differential transmission cross section is

$$\sigma(x_0, y_0, \Lambda) = \frac{1}{|J_\theta(x_0, y_0, \Lambda)|}, \tag{2}$$

where

$$J_\theta(x_0, y_0, \Lambda) = \partial_{x_0}\theta_x\partial_{y_0}\theta_y - \partial_{y_0}\theta_x\partial_{x_0}\theta_y \tag{3}$$

is the Jacobian of functions $\theta_x(x_0, y_0, \Lambda)$ and $\theta_y(x_0, y_0, \Lambda)$. Hence, equation

$$J_\theta(x_0, y_0, \Lambda) = 0 \tag{4}$$

gives the rainbow lines in the IP plane. The images of these lines determined by functions $\theta_x(x_0, y_0, \Lambda)$ and $\theta_y(x_0, y_0, \Lambda)$ are the rainbow lines in the TA plane.

The theory of crystal rainbows was employed to perform a detailed morphological study of the high-resolution channeling measurements using 2.0 MeV protons and a 55 nm thick (001) silicon membrane tilted away from the [001] direction [25]. It was proved that the doughnut effect was to be considered as the rainbow effect occurring with tilted crystals.

4. Interaction potentials

In the field of atomic collisions in solids, the ion–atom interaction potential is of the screened Coulomb type [9]. It can be expressed as $V(R) = V_0(R)\chi(R)$, where $V_0(R) = Z_1Z_2e^2/R$, Z_1 and Z_2 are the atomic numbers of the ion and crystal atom, respectively, e is the elementary charge, R is the ion–atom distance, and $\chi(R)$ is the ion–atom screening function, describing the effect of electron screening of the atomic nuclei. The screening function is determined using the Thomas–Fermi model or a Hartree–Fock method. In this study, we used the Molière's interaction potential [8], which had been derived from the Thomas–Fermi model, and the ZBL potential, which had been obtained applying an appropriate Hartree–Fock method to 261 atomic pairs [5–7]. The ZBL potential is often designated as the universal potential.

The screening function of the ZBL potential reads

$$\chi_{ZBL}(R) = \sum_{i=1}^{4}\alpha_i \exp\left(-\frac{\beta_i R}{a_{ZBL}}\right), \tag{5}$$

where

$$a_{ZBL} = \frac{(9\pi^2/128)^{1/3}}{Z_1^p + Z_2^p}a_0 \tag{6}$$

is the ZBL screening radius, a_0 is the Bohr radius, and $(\alpha_i) = (0.1818, 0.5099, 0.2802, 0.02817)$, $(\beta_i) = (3.2, 0.9423, 0.4028, 0.2016)$ and $p = 0.23$ are the fitting parameters [5–7].

The commonly used form of the screening function of the Molière's potential is

$$\chi_M(R) = \sum_{i=1}^{3}\gamma_i \exp\left(-\frac{\delta_i R}{a_F}\right), \tag{7}$$

where

$$a_F = \frac{(9\pi^2/128)^{1/3}}{\left(Z_1^{1/2} + Z_2^{1/2}\right)^{2/3}}a_0 \tag{8}$$

is the Firsov screening radius, and $(\gamma_i) = (0.10, 0.55, 0.35)$ and $(\delta_i) = (6, 1.2, 0.3)$ are the fitting parameters [8,29]. We denote it as the M(a_F) potential.

The parameters of the ZBL potential as well as of the M(a_F) potential were determined to make them accurate dominantly for small ion–atom distances. In analyzing their experimental results, Krause et al. [20] concluded that they were better reproduced by the Molière's potential with the Thomas–Fermi screening radius, being $a_{TF} = (9\pi^2/128)^{1/3}/Z_2^{1/3}a_0$, than by the M($a_F$) potential. We denote it as the M(a_{TF}) potential. This conclusion was attributed to the fact that each recorded angular distribution of transmitted ions was generated by the ions moving close to the channel axis, *i.e.*, far from the atomic strings defining the channel. One cannot expect a potential that has proven accurate close to the atoms of the strings, *i.e.*, for small ion–atom distances, like the ZBL or M(a_F) potential, to be accurate close to the channel axis, *i.e.*, for large ion–atom distances, where many atoms influence the ion propagation. The M(a_{TF}) potential can be written in a form depending on parameter a_F, rather than on a_{TF}, with parameters (δ_i) changed to $(\delta_i^c) = (\delta_i a_F/a_{TF})$. For $Z_1 = 1$ and $Z_2 = 14$, $(\delta_i^c) = (5.124, 1.025, 0.2562)$. We denote this potential as the M^c(a_F) potential.

The subject of this study is a sequence of high-resolution measurements performed with 2.0, 1.5, 1.0 and 0.7 MeV focused proton microbeams channeled in a 55 nm thick (001) silicon membrane. Fig. 1 shows the measured angular distributions of transmitted protons of energies of 2.0 and 0.7 MeV together with the corresponding distributions generated using a simulation code based

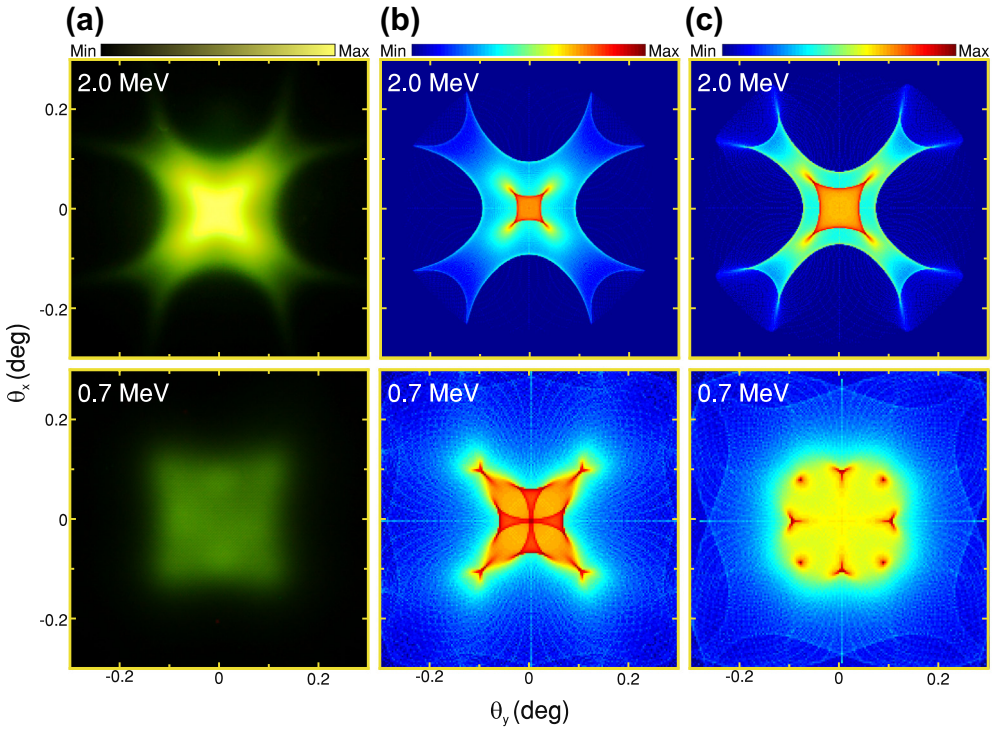

Fig. 1. (a) Experimental angular distributions of 2.0 and 0.7 MeV protons transmitted through a 55 nm thick (001) silicon membrane. (b) Corresponding theoretical distributions obtained with the ZBL interaction potential. (c) Corresponding theoretical distributions generated with the M(a_{TF}) potential.

on the continuum approximation [17] with two proton–atom interaction potentials – the ZBL and M(a_{TF}) potentials. The corresponding values of Λ calculated for the ZBL potential were 0.12 and 0.21, respectively. These experimental distributions, as well as the remaining ones given in Fig. 4b, were recorded by photographing a highly sensitive aluminum-coated YAG scintillator screen placed downstream of the crystal [22]. The technique did not make possible the extraction of accurate yields of transmitted protons along different lines on the screen in order to compare them to the corresponding theoretical yields. The only possibility was to compare the shapes and extents of the corresponding parts of the experimental and theoretical distributions, *i.e.*, to perform a morphological comparison of the distributions. The simulation code took into account the thermal vibrations of crystal atoms but not the collisions of protons with crystal electrons. We found that the contribution of the latter effect to the shapes of the distributions was minor. The number of atomic strings included in the calculations was 36, *i.e.*, we took into account the strings lying on the three nearest (relative to the channel axis) square coordination lines. The central part of each theoretical distribution obtained for an energy of 2.0 MeV is in the shape of a cusped square with four maxima lying on the apices of the cusps. However, the extent of this part of the distribution obtained with the M(a_{TF}) potential is larger than the extent of the part of the distribution generated with the ZBL potential. The central part of the corresponding experimental distribution also has the shape of a cusped square. Its extent is closer to the extent of the central part of the distribution generated with the M(a_{TF}) potential. The peripheral part of each theoretical distribution obtained for this energy has the shape of a line with four pairs of cusps. The extent of the peripheral part of the corresponding measured distribution is closer to the extent of the peripheral part of the distribution obtained with the ZBL potential.

The theoretical distribution depicted in Fig. 1 obtained for a proton energy of 0.7 MeV with the ZBL potential also has the shape of a cusped square with four maxima lying on the apices of the cusps. In addition, it has an internal structure composed of four cusped isosceles triangles joined at the origin with four pairs of maxima lying on the apices of the peripheral cusps and a maximum at the origin. The corresponding theoretical distribution generated with the M(a_{TF}) potential has approximately the shape of a square with four stronger maxima lying on lines $\theta_x = 0$ and $\theta_y = 0$, and four weaker ones lying on lines $\theta_y = \pm\theta_x$. The corresponding experimental distribution has approximately the shape of a square too, being closer to the theoretical distribution obtained with the M(a_{TF}) potential. Also, it does not have a maximum at the origin, like the theoretical distribution obtained with the M(a_{TF}) potential and unlike the distribution generated with the ZBL potential.

On the basis of these comparisons, we assume that we can modify the M^c(a_F) potential and make it accurate close to the channel axis but without compromising its accuracy close to the atomic strings. We shall construct such a potential and employ it for analysis of the above mentioned sequence of high-resolution channeling measurements. The construction will be based on adjusting the shapes of the rainbow lines in the TA plane by a minimal modification of the M^c(a_F) potential. This decision is based on the well-established morphological fact that an angular distribution of transmitted ions, generated for a proton energy, crystal thickness and crystal tilt angle, and its evolution with these parameters are fully determined by the associated rainbow pattern in the TA plane and its evolution [17,18,25]. The resulting potential will be denoted as the rainbow potential. Fig. 2 gives the dependences of the ZBL and M(a_{TF}) potentials on the proton–atom distance. The inset shows the three components of the M^c(a_F) potential, to be modified in order to obtain the rainbow potential.

The construction of the rainbow potential is performed for a proton energy of 2.0 MeV since in this case, two well-separated rainbow lines appear in the IP plane [25]. This is shown in Fig. 3a for the ZBL and M(a_{TF}) potentials. The lines were calculated applying the continuum approximation with the thermal vibrations of

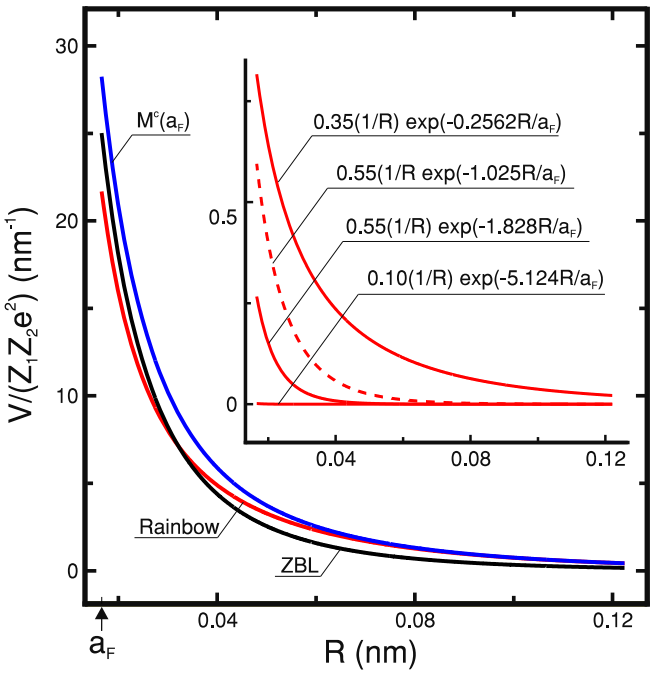

Fig. 2. Dependences of the ZBL, M(a_{TF}) and rainbow interaction potentials on the proton–atom distance – black, blue and red lines, respectively. Inset: the components of the M^c(a_F) potential and the second component of the rainbow potential as functions of the proton–atom distance. (For interpretation of the references to color in this figure legend, the reader is referred to the web version of this article.)

crystal atoms included [17]. The number of atomic strings included in the calculations was 36. The first line lies close to the channel center and the second one close to the atomic string. The associated rainbow lines in the TA plane are depicted in Fig. 3b. We emphasize that the crystals used by Krause et al. [19,20] were not sufficiently thin for two such lines to occur in the IP plane. We now focus on points 1 and 2 in the IP plane, belonging to the first and second rainbow lines, and on points 1′ and 2′ in the TA plane, being the images of points 1 and 2, respectively. Analysis showed that the positions of points 1′ and 2′ were not sensitive to changes of parameter δ_1^c, were sensitive to changes of parameter δ_2^c, and were very sensitive to changes of parameter δ_3^c. Taking those findings into account, we chose to keep parameters (γ_i), δ_1^c and δ_3^c fixed and change parameter δ_2^c with the objectives of: (i) moving point 1′ corresponding to the M^c(a_F) potential to minimize its distance from point 1′ corresponding to the M(a_{TF}) potential, and (ii) moving point 2′ corresponding to the M^c(a_F) potential to minimize its distance from point 2′ corresponding to the ZBL potential. In fact, we minimized the sum of squares of the relative distances between points 1′ and between points 2′. As a result, parameter δ_2^c was modified from 1.025 to 1.828. The corresponding component of the rainbow potential is given in the inset of Fig. 2. Thus, the rainbow potential is defined by Eqs. (7) and (8) with parameters (δ_i) replaced by (δ_i^r) = (5.124, 1.828, 0.2562). This potential is presented in Fig. 2, and the associated rainbow lines in the IP and TA planes are shown in Fig. 3a and b, respectively. The first rainbow line in the TA plane generated with the rainbow potential practically coincides with the first rainbow line generated with the M(a_{TF}) potential, and the second rainbow line in this plane obtained with the rainbow potential is very close to the second rainbow line obtained with the ZBL potential.

One should mention here that if the adjusting of the shapes of the rainbow lines in the TA plane were performed differently, *e.g.*, by changing more than one parameter of the M^c(a_F) potential, the resulting rainbow potential would be different. However, our current experience in applying the method tells that these differences are minor.

Fig. 4a and b depict the rainbow patterns in the IP and TA planes for proton energies of 2.0, 1.5, 1.0 and 0.7 MeV obtained with the rainbow potential, respectively. The corresponding values of Λ were 0.16, 0.19, 0.23 and 0.28. The patterns were calculated applying the continuum approximation with the thermal vibrations of crystal atoms included [17]. The number of atomic strings included

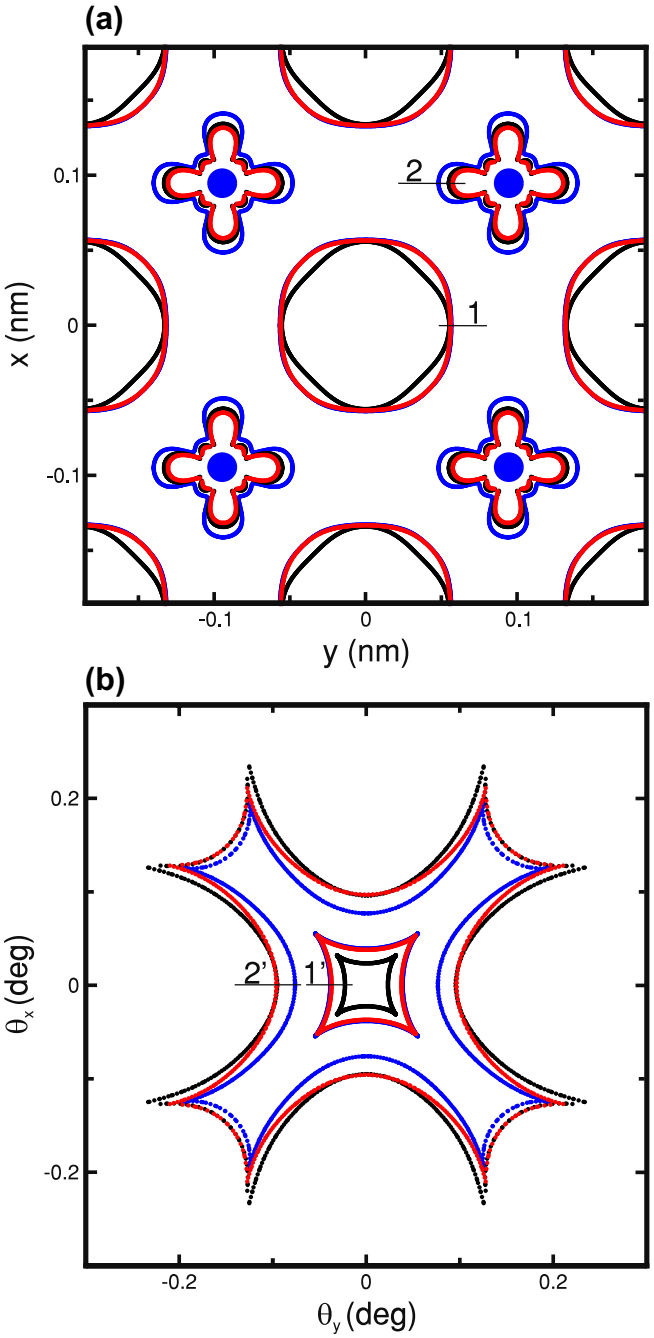

Fig. 3. (a) Rainbow patterns in the IP plane for 2.0 MeV protons transmitted through a 55 nm thick (001) silicon membrane for the ZBL, M(a_{TF}) and rainbow interaction potentials – black, blue and red lines, respectively; the blue line close to the origin is covered by the red line. The blue full circles represent the atomic strings. (b) Associated rainbow patterns in the TA plane; the blue line close to the origin is covered by the red line. (For interpretation of the references to color in this figure legend, the reader is referred to the web version of this article.)

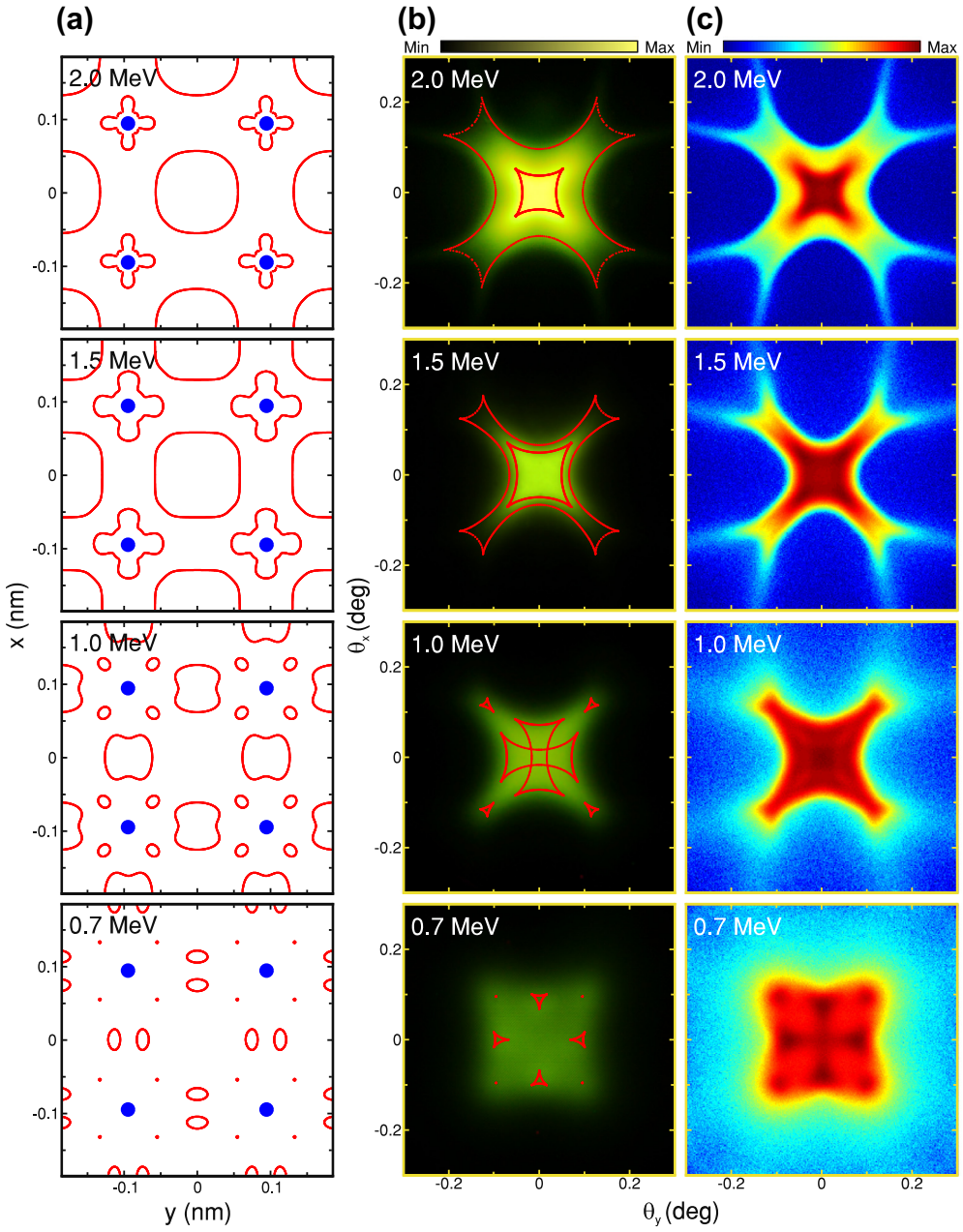

Fig. 4. (a) Rainbow patterns in the IP plane for 2.0, 1.5, 1.0 and 0.7 MeV protons transmitted through a 55 nm thick (001) silicon membrane generated with the rainbow interaction potential. (b) Corresponding experimental angular distributions of transmitted protons and the associated rainbow patterns in the TA plane. (c) Corresponding theoretical distributions generated using the FLUX simulation code with the rainbow potential.

in the calculations was 36. As already stated, for an energy of 2.0 MeV, there are two rainbow lines in the IP plane, lying close to the channel center and close to the atomic string. The associated rainbow pattern in the TA plane comprises a cusped square, being the image of the rainbow line in the IP plane close to the channel center, and a line with four pairs of cusps, being the image of the rainbow line in the IP plane close to the atomic string. The rainbow patterns in the IP and TA planes for an energy of 1.5 MeV are similar to those for an energy of 2.0 MeV with the rainbow lines in both planes lying closer to each other. The rainbow pattern in the IP plane for an energy of 1.0 MeV contains six lines. There are two equivalent quasi-rectangular lines connecting the neighboring channels, *i.e.*, lying across the channel walls, and four equivalent quasi-elliptical lines lying close to the atomic string. There is no line around the channel center. The associated rainbow pattern in the TA plane contains two crossed cusped rectangular lines, being the images of the two quasi-rectangular lines in the IP plane, and four cusped isosceles triangles, being the images of the four quasi-elliptical lines in the IP plane. For an energy of 0.7 MeV, there are two equivalent pairs of quasi-elliptical rainbow lines in the IP plane lying in the neighboring channels close to the channel walls and four equivalent rainbow points in the IP plane lying close to the atomic string. Again, there is no line around the channel center. The associated rainbow pattern in the TA plane comprises four cusped isosceles triangles, being the images of the two pairs of quasi-elliptical lines in the IP plane, and four rainbow points, being the images of the four points in the IP plane. In all these cases, the inner side of each rainbow line in the TA plane is the bright side of the rainbow while its outer side is the dark side of the rainbow. It should be mentioned that for an energy of 0.7 MeV, there is no line

in the TA plane around the origin, which explains the above mentioned fact that the corresponding experimental distribution does not have a maximum at the origin.

Fig. 4b also gives the experimental angular distributions of transmitted protons for energies of 2.0, 1.5, 1.0 and 0.7 MeV. The corresponding rainbow patterns generated with the rainbow potential fully determine the distributions – they appear as the "skeletons" of the distributions. A careful inspection and comparison of the measured distributions and rainbow patterns demonstrated excellent agreement, in spite of the fact that the rainbow patterns were obtained using the continuum approximation [2] with the thermal vibrations of crystal atoms included but with the focusing of the incident proton beam, the collisions of protons with crystal electrons, and crystal defects neglected. Fig. 4c depicts the corresponding distributions generated using the FLUX simulation code [27,28] with the rainbow potential. The number of atomic strings included in the calculations was 36. A comparison of the measured and simulated distributions also demonstrated excellent agreement. The simulated distributions did not take into account the focusing of the incident proton beam and crystal defects. On the basis of these comparisons, we concluded that the above made assumption on the possibility of modification of the $M^c(a_F)$ potential for protons transmitted through a silicon crystal was proven.

Let us complete the study with an analysis of five typical trajectories of transmitted protons for an energy of 2.0 MeV calculated for the rainbow potential. The initial points of two of these trajectories, designated as trajectories I and II, were chosen to lie on the rainbow line close to the channel center, and the initial points of the remaining three of them, designated as trajectories III, IV and V, on the rainbow line close to the atomic string. The projections of these trajectories on the *xz* and *yz* planes are given in Fig. 5a and b, respectively. The inset of Fig. 5b depicts the initial points of the trajectories. The analysis showed that trajectories I, II and III included one deflection from a channel wall, and that trajectories IV and V included two deflections from the walls. We analyzed the other trajectories of transmitted protons as well. The conclusion of the whole analysis was that the trajectories of about 90% of all the protons transmitted through the crystal included one deflection from a channel wall, and that the trajectories of the remaining about 10% of them, whose initial points lied very close to the atomic string, included two deflections from the walls. An analysis of the typical trajectories of transmitted protons for energies of 1.5, 1.0 and 0.7 MeV calculated for the rainbow potential gave similar results, but, as expected, with the percentage of trajectories of all the transmitted protons that included one deflection from a channel wall being lower for a lower energy.

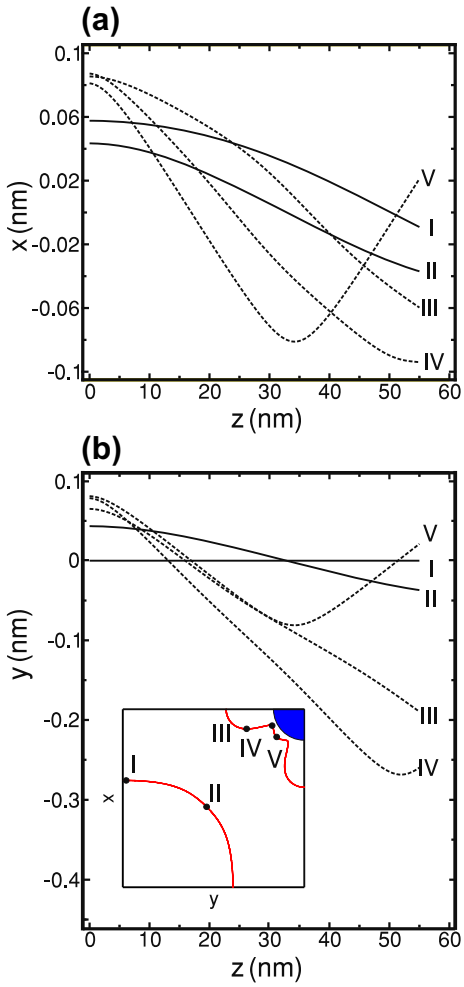

Fig. 5. (a) Projections of five typical trajectories of 2.0 MeV protons transmitted through a 55 nm thick (001) silicon membrane on the *xz* plane calculated for the rainbow interaction potential. (b) Associated projections of the proton trajectories on the *yz* plane. Inset: the initial points of the proton trajectories.

5. Summary

This morphological method of modifying the $M^c(a_F)$ potential can be applied in each case of ion transmission through axial channels of a thin crystal where the rainbow pattern in the IP plane contains a line close to the channel center and a line close to the atomic string. Such a case can always be prepared by changing the ion energy or crystal thickness. The adjusted rainbow pattern in the TA plane fully determines the associated angular distribution of transmitted ions, generated with the resulting rainbow potential. This distribution ought to be compared with the corresponding distribution obtained in a high-resolution measurement. If they agree, one can conclude that a very accurate interaction potential has been extracted from this measurement. This potential should also be very accurate for other values of ion energy and crystal thickness [5–7]. Unlike the ZBL, $M(a_F)$ and $M(a_{TF})$ potentials, it will be accurate across the whole channel.

If this method is applied to different axial channels of a thin crystal, it will be possible to deduce an average rainbow potential to accurately simulate the ion penetration through a randomly oriented crystal of the same atomic composition.

This method may be applied in analogous ways in other fields where the rainbow effect occurs and plays an important role, *i.e.*, to nucleus-nucleus collisions [30–32], atom, ion or electron collisions with atoms or molecules [33,34], and atom, ion or electron scattering from crystal surfaces [35–39]. That would lead to more accurate interaction potentials in these fields. It should be mentioned that a similar approach to atom scattering from crystal surfaces has already produced important results [40,41].

Acknowledgment

S. P., N. N. and M. Ć. acknowledge the support to this work provided by the Ministry of Education, Science and Technological Development of Serbia through project *Physics and Chemistry with Ion Beams*, No. III 45006.

References

[1] M.T. Robinson, O.S. Oen, Phys. Rev. 132 (1963) 2385.
[2] J. Lindhard, K. Dan. Vidensk. Selsk., Mat.-Fys. Medd. 34 (14) (1965) 1.
[3] J.H. Barrett, Phys. Rev. B 3 (1971) 1527.

[4] D.S. Gemmell, Rev. Mod. Phys. 46 (1974) 129.
[5] J.F. Ziegler, J.P. Biersack, U. Littmark, The Stopping and Range of Ions in Solids, Pergamon Press, New York, 1985.
[6] J.F. Ziegler, J.P. Biersack, M.D. Ziegler, SRIM – The Stopping and Range of Ions in Matter, SRIM, Annapolis, 2008.
[7] J.F. Ziegler, M.D. Ziegler, J.P. Biersack, Nucl. Instr. Meth. Phys. B 268 (2010) 1818.
[8] G. Molière, Z. Naturforsch. A 2 (1947) 133.
[9] M. Nastasi, J.W. Mayer, Ion Implantation and Synthesis of Materials, Springer-Verlag, Berlin, 2006.
[10] R.W. Hamm, M.E. Hamm (Eds.), Industrial Accelerators and Their Applications, World Scientific, Singapore, 2012.
[11] B. Schmidt, K. Wetzig (Eds.), Ion Beams in Materials Processing and Analysis, Springer-Verlag, Berlin, 2013.
[12] M.B.H. Breese, D.N. Jamieson, P.J.C. King, Materials Analysis Using a Nuclear Microprobe, John Wiley & Sons, New York, 1996.
[13] N. Nešković, Phys. Rev. B 33 (1986) 6030.
[14] N. Nešković, B. Perović, Phys. Rev. Lett. 59 (1987) 308.
[15] H.M. Nussenzveig, Diffraction Effects in Semiclassical Scattering, University Press, Cambridge, 1992.
[16] J.A. Adam, Phys. Rep. 356 (2002) 229.
[17] S. Petrović, L. Miletić, N. Nešković, Phys. Rev. B 61 (2000) 184.
[18] N. Nešković, S. Petrović, Nanosci. Nanotechnol. Lett. 4 (2012) 1033.
[19] H.F. Krause, S. Datz, P.F. Dittner, J. Gomez del Campo, P.D. Miller, C.D. Moak, N. Nešković, P.L. Pepmiller, Phys. Rev. B 33 (1986) 6036.
[20] H.F. Krause, J.H. Barrett, S. Datz, P.F. Dittner, N.L. Jones, J. Gomez del Campo, C.R. Vane, Phys. Rev. A 49 (1994) 283.
[21] J.H. Barrett, Nucl. Instr. Meth. Phys. B 44 (1990) 367.
[22] Z.Y. Dang, M. Motapothula, Y.S. Ow, T. Venkatesan, M.B.H. Breese, M.A. Rana, A. Osman, Appl. Phys. Lett. 99 (2011) 223105.
[23] M. Motapothula, Z.Y. Dang, T. Venkatesan, M.B.H. Breese, M.A. Rana, A. Osman, Nucl. Instr. Meth. Phys. B 283 (2012) 29.
[24] M. Motapothula, Z.Y. Dang, T. Venkatesan, M.B.H. Breese, M.A. Rana, A. Osman, Phys. Rev. Lett. 108 (2012) 195502.
[25] M. Motapothula, S. Petrović, N. Nešković, Z.Y. Dang, M.B.H. Breese, M.A. Rana, A. Osman, Phys. Rev. B 86 (2012) 205426.
[26] M. Motapothula, Z.Y. Dang, T. Venkatesan, M.B.H. Breese, Nucl. Instr. Meth. Phys. B 330 (2014) 24.
[27] P.J.M. Smulders, D.O. Boerma, Nucl. Instr. Meth. Phys. B 29 (1987) 471.
[28] P.J.M. Smulders, D.O. Boerma, M. Shaanan, Nucl. Instr. Meth. Phys. B 45 (1990) 450.
[29] O.B. Firsov, Sov. Phys., J. Exp. Theor. Phys. 5 (1957) 1192.
[30] K.W. McVoy, H.M. Khalil, M.M. Shalaby, G.R. Satchler, Nucl. Phys. A 455 (1986) 118.
[31] F. Michel, G. Reidemeister, S. Ohkubo, Phys. Rev. Lett. 89 (2002) 152701.
[32] D.T. Khoa, W. von Oertzen, H.D. Bohlen, S. Ohkubo, J. Phys. G: Nucl. Part. Phys. 34 (2007) R111.
[33] J.N.L. Connor, D. Farelly, J. Chem. Phys. 75 (1981) 2831.
[34] G. Ziegler, M. Rädle, O. Pütz, K. Jung, H. Ehrhardt, K. Bergmann, Phys. Rev. Lett. 58 (1987) 2642.
[35] A.W. Kleyn, T.C.M. Horn, Phys. Rep. 199 (1991) 191.
[36] C.O. Reinhold, J. Burgdörfer, K. Kimura, H. Mannami, Phys. Rev. Lett. 73 (1994) 2508.
[37] D.M. Danailov, D.J. O'Connor, K.J. Snowdon, Surf. Sci. 347 (1996) 215.
[38] H. Winter, Phys. Rep. 367 (2002) 387.
[39] S. Miret-Artés, E. Pollak, Surf. Sci. Rep. 67 (2012) 161.
[40] P. Tiwald, A. Schüller, H. Winter, K. Tökesi, F. Aigner, S. Gräfe, C. Lemell, J. Burgdörfer, Phys. Rev. B 82 (2010) 125453.
[41] U. Specht, M. Busch, J. Seifert, A. Schüller, H. Winter, Phys. Rev. B 84 (2011) 125440.